Effects of Average Flow Stress and Energy Density on Quality and Properties of Friction Stir Welded Aluminum

Kevin Colligan and Jonathon Hunt
Concurrent Technologies Corporation
Johnstown, PA USA

Abstract

The results of an ongoing program to develop advanced controls techniques for friction stir welding are presented. New data features, derived from the basic details of the welding process, were conceived and tested as expressions of real-time process conditions. Two such data features, average flow stress and energy density, were found to be particularly useful for controlling weld quality in terms of weld soundness and mechanical properties. This paper proposes these data features, along with weld pitch, as a method for specification of welding procedures in a way that is adaptive to welding conditions for complex applications where procedures based on fixed machine settings are not adequate.

Introduction

This work is part of an ongoing program to facilitate the adoption of friction stir welding (FSW) for the construction of military ground vehicles, primarily those constructed from aluminum. Employing a relatively new joining process on a large procurement program presents many challenges, such as impacts on product design, development of facilities and workforce, and qualification of procedures. One key barrier to adoption has been the lack of on-staff experience with the process at all levels. The present program seeks to simplify weld qualification and reduce operator skill requirements by developing "smarter" welding control systems. The program has followed two parallel paths to achieve this. One path, pursued by PAR Systems (Eden Prairie, MN, USA), was to develop machine learning techniques and new sensor technologies which could improve the ability of a welding system to adapt to process conditions. In parallel, Concurrent Technologies Corporation (CTC) followed the approach of developing advanced control techniques that use conventional force sensor data and new process knowledge to monitor the process and adapt to changing conditions.

Traditional methods for weld qualification, largely based on arc welding processes, seek to control weld quality by specifying nominal values and ranges for all variables that influence weld quality. Friction stir welding differs from arc welding processes in its inherent sensitivity to thermal conduction boundary conditions. This dependence makes it necessary to qualify welding in all thermal boundary conditions on a production assembly to be certain of quality control. These boundary conditions include workpiece, anvil and fixture geometry, often requiring the development of customized sequences of machine settings to accommodate geometry changes. Other process influences produce weld-to-weld variability, including workpiece and fixture initial temperature, workpiece fit-up and workpiece-to-fixture contact conditions. These factors make the traditional qualification of welding procedures for large, complex structures difficult and expensive to develop, and combined with in-process variability, it likely does a poor job of ensuring weld properties.

Adaptive control of FSW seeks to solve these problems by using real-time sensor data to guide manipulation of the basic machine settings along the length of a weld to hold process conditions constant, adapting to changes in workpiece and fixture geometry and to in-process variability. The most successful technique used in the past has been control based on welding tool temperature, either by manipulating the spindle speed or the spindle torque. Closed-loop temperature control using an instrumented welding tool has been demonstrated to precisely regulate the welding tool temperature, which is reflective of heat generation by the process [1-6]. Using this method, a welding system can avoid producing some types of defects by manipulating the basic machine settings, thereby maintaining a constant welding tool temperature. Some recent force-based methods have been developed which rely on time-domain analysis to infer the production of defects, while other methods used frequency-domain analysis for this purpose, correlating the low-frequency content of lateral force measurements with defect production [7-11]. These methods were generally used for analyzing "cold" welding conditions, where wormhole defects were produced, and were used for detecting defect formation rather than for avoiding it.

Spindle torque has only recently been directly correlated with weld quality [12-17]. In prior work at CTC [12-15], the spindle torque was used to calculate an average flow stress at the tool/workpiece interface, which was then correlated with weld quality. The use of flow stress instead of torque was based on the notion that local conditions might be the root cause of some welding defects, so expressing the torque in terms of force per unit area might reveal a quality indicator that was independent of tool geometry and workpiece thickness. Rodrigues, et al, [16] related weld defect formation to specific energy, calculated from spindle torque, spindle speed and welding speed. Liu, et al, [17] studied defect formation in three alloys as a function of temperature, torque, power and heat input (specific energy), and concluded that low power output was necessary for sound weld formation in the range of parameters tested.

The present work seeks to provide a method of manipulating machine settings in real time to avoid defect formation using the basic force and spindle torque measurements that are commonly available on modern welding systems, obviating the need for instrumenting the welding tool. New data features were developed to express welding conditions, such as unit contact force (flow stress), heat flux (power/area) and energy density (energy/volume), in ways that are more meaningful than the constituent quantities. Referred to as unit-area analysis, the method normalizes the expression of welding conditions with respect to thickness by relating conditions to units of area at the tool/workpiece interface surface.

Unit-area analysis was used in two ways on this program. Initial experiments consisted of bead-on-plate welds in constant-width plates that represented approximately constant boundary conditions. The range of machine settings used was scaled to produce defects from "hot" and "cold" conditions. Defect morphology was documented and the unit-area quantities were correlated with those indications. Analysis was performed to explore the effect of machine settings and workpiece thickness on these features. The second application for unit-area analysis involved identification of correlations between the data features and weld quality and strength, which led to the postulation of control algorithms to modify the machine settings to avoid defect production, described in a subsequent paper [18]. The present paper describes the analysis of constant boundary condition welds and the correlation between unit-area quantities, specifically, flow stress, energy density and weld pitch, and joint quality and properties.

Background

The technical basis for unit-area analysis has been published previously [12-15] but will be briefly repeated here for completeness. The analysis depends on reducing the welding tool geometry to the first moment of area, referred to as G (for geometry) [18], calculated as the integral of the radius over the tool/workpiece interface area. The expression of G is dependent on the style of welding tool used. For example, for a flat or tapered shoulder tool with a flat-tipped, frustum-shaped probe, the expression for G is,

$$G = \frac{2\pi}{3}\left[\frac{S^3 - {P_r}^3}{\cos\alpha} + \frac{t((P_R + P_T)^2 - P_R P_T)}{\cos\beta} + {P_T}^3\right] \quad (1)$$

where,

$\alpha = shoulder\ concavity\ angle$
$\beta = frustum\ probe\ half\ angle$
$S = shoulder\ radius$
$P_R = probe\ root\ radius$
$P_T = probe\ tip\ radius$
$r = dimension\ in\ radial\ direction$
$z = dimension\ along\ probe\ axis$
$t = workpiece\ thickness, or\ probe\ length$
$\theta = anglular\ position$

To express the rotational speed of different welding tools on an equal basis it is necessary to convert spindle speed to average surface velocity, expressed as,

$$\omega\bar{r} = \omega\frac{G}{total\ area} \quad (2)$$

where ω is the angular velocity, r̄ is the centroid radius and 'total area' refers to the tool/workpiece interface area.

To express welding speed, it has been found that the most useful terms are the conventional expression in terms of length per unit time, or in some applications, in terms of weld pitch, expressed as length per revolution,

$$weld\ pitch = \frac{v}{2\pi\omega} = \frac{welding\ speed}{spindle\ speed} \quad (3)$$

The unit-area data features presented here are flow stress, energy density, heat flux, shoulder pressure and lateral pressure. Flow stress represents the average of the distributed contact shear stress over the tool/workpiece interface, conventionally expressed as a normal stress [20], and is expressed as,

$$\sigma_{flow} = \frac{T\sqrt{3}}{G} \quad (4)$$

where T is the spindle torque. The heat flux, ϕ_q, with units of power per unit area, is calculated as,

$$\phi_q = \frac{T}{G} \times \omega \bar{r} \tag{5}$$

Early research in FSW attempted to normalize heat input based on the total power output and the welding speed, yielding "specific energy" which represented the energy per unit length of weld [21]. However, this formulation did not account for differences with respect to workpiece thickness. To improve the expression of the energy put into the workpiece, in terms of volume of processed material, the energy density can be calculated as the heat flux divided by the travel speed, or,

$$\rho_E = \frac{\phi_q}{travel\ speed} = \frac{2\pi T}{weld\ pitch \times total\ tool\ area} \tag{6}$$

It is notable that holding constant spindle torque and weld pitch has the effect of fixing the energy density. Two other unit-area quantities are used to normalize the plunge force and the lateral force. The shoulder pressure, SP, is simply the plunge force divided by the shoulder area,

$$\text{SP} = \frac{F_{plunge}}{\pi S^2} \tag{7}$$

The lateral pressure is expressed as the lateral force divided by the lateral area of the probe. For a frustum-shaped probe with a flat tip, the lateral pressure is,

$$\text{LP} = \frac{\sqrt{\left({F_{longitudinal}}^2 + {F_{transverse}}^2\right)}}{t * (P_r + P_t)/2} \tag{8}$$

where $F_{longitudinal}$ and $F_{transverse}$ are the longitudinal and transverse forces on the welding tool, respectively.

Approach

The results presented are from welds made in 50.8-mm, 25.4-mm and 12.7-mm 7075-T6 aluminum plates using welding tools with flat, scrolled shoulders and frustum-shaped pins with threads and flats, as summarized in Table 1. A limited set of welds in 12.7-mm 6061-T6 aluminum plates were also made at CTC. Welds were made at Concurrent Technologies Corporation (CTC, Johnstown, PA, USA) and at PAR Systems (Eden Prairie, MN, USA), as indicated in the table. The welding conditions represented a broad range of welding speed and spindle speed values, intended to produce welds with a range of quality. For most experimental runs, the weld was divided into multiple segments of stable machine settings. The plunge force on welds made at CTC was manipulated to give constant shoulder contact conditions, as determined by visual monitoring and manual manipulation in load or position control. The targeted shoulder contact condition was full shoulder contact with minimal excess flash. The welds made at PAR were all made in plunge force control. Each segment was subjected to phased array ultrasonic testing (PAUT), visual inspection of the weld crown, transverse tensile testing and macro section inspection. The data from each segment was averaged to generate a single data vector for subsequent analysis. The calculated unit-area quantities included surface velocity, flow stress, energy density, heat flux, shoulder pressure and lateral probe pressure. The data and post-weld inspections were analyzed to identify trends and to correlate unit-area data features with post-weld inspection results.

Table 1. Welding tools for 50.8-mm, 25.4-mm and 12.7-mm welds.

Workpiece thickness, mm	50.8-mm (CTC)	25.4-mm (CTC)	12.7-mm (CTC)	12.7-mm (PAR)
Shoulder diameter, mm	47.0	35.6	30.5	28.6
Probe root diameter, mm	24.2	21.0	12.5	12.7
Probe tip diameter, mm	11.8	12.7	9.5	9.6
Probe length, mm	49.1	24.7	12.0	12.2
Shoulder style	Flat, scrolled			
Shoulder number of scrolls	3	3	3	3
Probe style	Frustum, threads and flats			
Thread pitch, mm/thread	1.81	1.81	1.81	1.50
Number of probe flats	5	5	4	3

Results

The results were analyzed with two main objectives. First, an effort was made to analyze the data to permit an empirical expression for prediction of flow stress from the machine settings for welds in 7075-T6 with constant boundary conditions in a way that was independent of workpiece thickness. The purpose was to determine the essential data features related to welding conditions at the tool/workpiece interface. The second objective was to correlate unit-area data features with weld quality. The purpose there was to facilitate the development of automatic controls that could manipulate the basic machine settings in real time to avoid the production of defects, even in conditions of variable boundary conditions.

The analysis of flow stress with respect to basic machine settings (spindle speed, welding speed and plunge force) was conducted to assess the utility of unit-area data features for normalizing the data from different workpiece thickness and to document the relationships between variables. The conventional means of expressing the relationship between spindle torque and machine settings is to simply plot the torque as a function of spindle speed, as shown on the left side in Figure 1. In this series, welds were made in 12.7-mm and 25.4-mm 7075-T6 aluminum plates with experimental runs planned to produce welds at different surface velocity levels with similar weld pitch values. As can be seen in the figure, the torque data is dominated by the thickness difference, making it difficult to consider other effects. On the chart on the right side of the figure, torque is converted to average flow stress using equation (4), which normalizes the torque with respect to thickness using parameter G, the first moment of area of each welding tool. The spindle speed is converted to average surface velocity to compensate for differences in tool diameter.

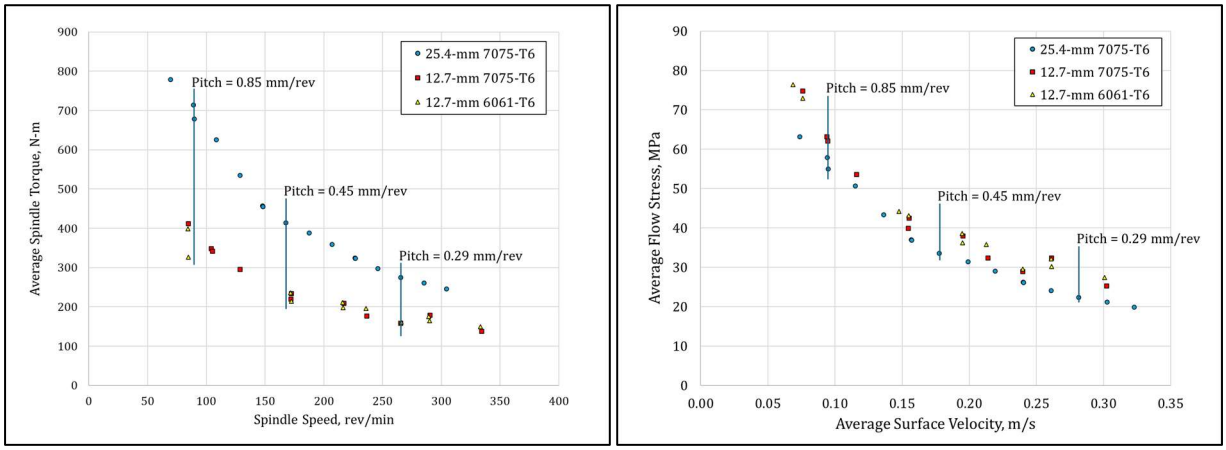

Figure 1. Spindle torque and flow stress, welds with similar weld pitch values, 25.4-mm thick plates welded at 1.27 mm/s, 12.7-mm thick plates welded at 1.48 mm/s.

The data plotted in Figure 2 shows differences between flow stress data plotted as a function of the inverse of the surface velocity, comparing welds made with similar weld pitch on the left and welds made with similar welding speed on the right. Comparing these charts, it appears that analyzing the flow stress with respect to welding speed produces better normalization with respect to thickness when comparing welds with similar welding speed rather than similar weld pitch. This observation specifically applies to the welds made with constant shoulder contact conditions, as was the case in the welds made at CTC, since plunge force is related to weld pitch and to flow stress, making it necessary to include weld pitch in a comprehensive study of flow stress as it relates to machine settings, addressed below. Similar analyses are possible with respect to the other unit-area data features, such as energy density.

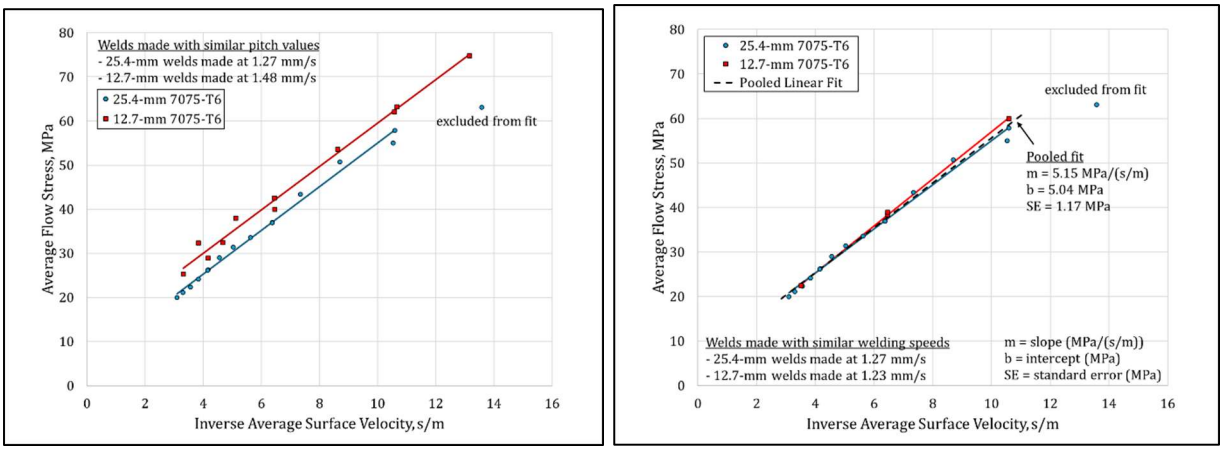

Figure 2. Average flow stress as a function of inverse surface velocity, 25.4-mm and 12.7-mm 7075-T6 FSW, (left) welds with similar pitch values and (right), welds with similar welding speed.

The experimental results can be used to develop more comprehensive empirical expressions that relate the average flow stress to the welding tool geometry and machine settings. The pool of data from 151 welding conditions was analyzed using multiple linear regression with flow stress as the dependent variable and weld pitch, welding speed, inverse surface velocity and shoulder pressure as independent variables. Figure 3 shows the flow stress calculated from torque measurements as a function of the predicted value for the four cohorts from this study, including welds in 50.8-mm,

25.4-mm and 12.7-mm welds in 7075-T6 produced at CTC and welds in 12.7-mm 7075-T6 produced at PAR Systems. The root-mean-squared-error (RMSE) was about 3.2 MPa, which may not be sufficiently precise as a predictive tool. Much better results were obtained by using the linear regression on each individual cohort separately or by pooling results from the 50.8-mm and 25.4-mm welds and separately pooling the results from 12.7-mm welds, as shown in Figure 4. Here, RMSE values were much smaller, demonstrating the characterization of the relationship between flow stress and tool geometry and machine settings. The linear regression results are summarized in Table 2. Including weld pitch as an effect in the linear regression is essentially the same as including an interaction effect between welding speed and inverse surface velocity.

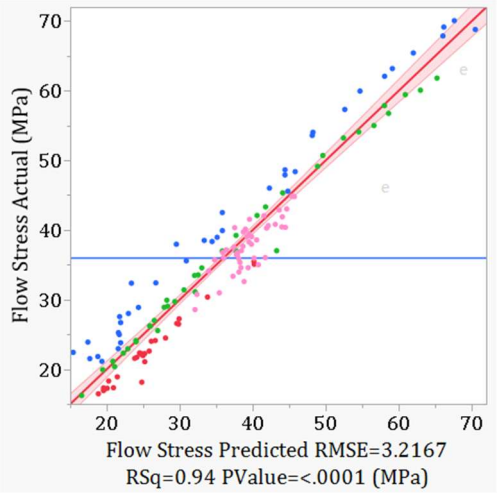

Figure 3. Linear regression results, flow stress as a function of weld pitch, shoulder pressure, welding speed and inverse surface velocity, 50.8-mm (CTC, red), 25.4-mm (CTC, green) and 12.7-mm (CTC, blue, and PAR, pink) 7075-T6 FSW, 151 welding conditions, no replicates.

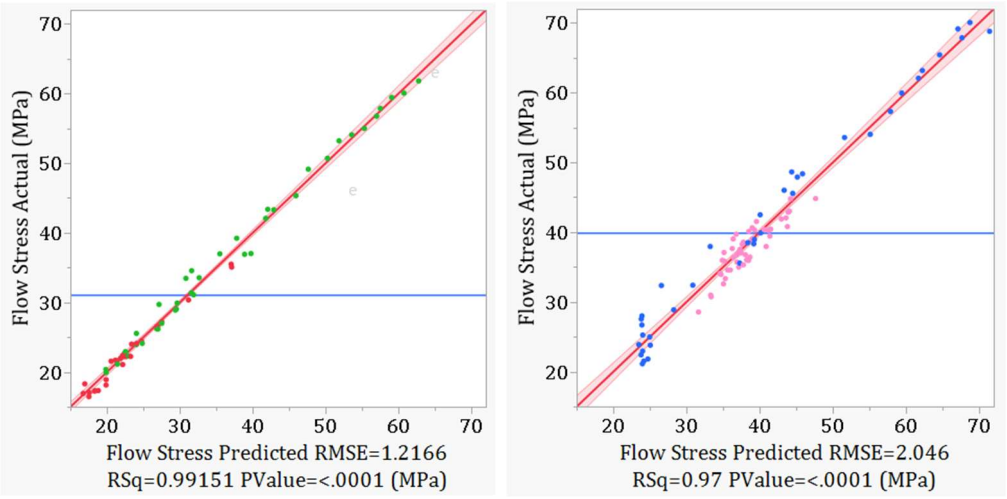

Figure 4. Linear regression results, flow stress as a function of weld pitch, shoulder pressure, welding speed and inverse surface velocity, (left) 50.8-mm (red) pooled with 25.4-mm (green), (right) 12.7-mm (CTC, blue, PAR, pink), 7075-T6 FSW.

Table 2. Linear regression results from analysis of flow stress as a function of inverse surface velocity, welding speed, shoulder pressure and weld pitch, 7075-T6 FSW.

Thickness	Intercept	Coefficients			
		Inverse Surface Velocity	Welding Speed	Shoulder Pressure	Weld Pitch
(mm)	(MPa)	(MPa/(m/s))	(MPa/(m/s)	(MPa/MPa)	(MPa/(mm/rev)
50.8, 25.4 and 12.7	-0.78	2.88	-5.23	0.24	21.89
50.8 and 25.4	-6.07	2.51	-6.38	0.41	21.21
12.7 (CTC + PAR)	11.84	3.29	-4.75	0.04	22.28
25.4 (12 welds)	-3.45	3.69	0.67	0.19	9.74

The linear regression method can also be used to analyze continuous log file data, with each row treated as a data vector. The log files from 12 welds in 25.4-mm 7075-T6 were pooled and analyzed to produce a prediction expression from 56,955 data vectors. Figure 5 shows the actual flow stress plotted against the predicted values and the parameters for the prediction expression are listed in Table 2. These welds all had constant boundary conditions and multiple segments of stable machine settings. However, the shoulder contact conditions were not all the same, with some welds having some amount of excess flash production. Two welds had sections that exhibited very heavy flash which influenced the resulting correlation, with actual flow stress significantly lower than the prediction, so those segments were excluded from the analysis. For each weld, the first and last 75 mm of weld were also excluded. It is notable that the cluster of data along linear trend in the figure is bordered above and below by transient effects arising from sudden spindle speed changes, produced when the spindle speed was suddenly changed to transition machine settings between segments. It is also interesting that at the highest flow stress tested, about 70 MPa, the actual torque values were lower than the prediction, suggesting a change in the underlying process.

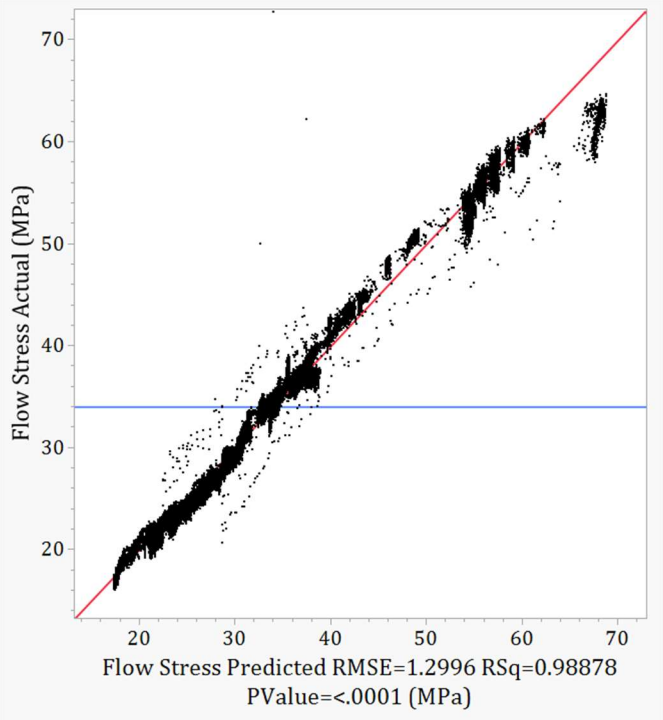

Figure 5. Linear regression results, flow stress as a function of weld pitch, shoulder pressure, welding speed and inverse surface velocity, continuous log file data from 12 welds in 25.4-mm 7075-T6 aluminum.

Flow stress and weld pitch were found to correlate with weld quality in terms of the production of volumetric defects. Figure 6 shows examples of two types of defects observed, each produced by different mechanisms. The image on the left shows volumetric defects associated with the boundary of the stir zone at the weld root and on the upper, advancing side. These defects developed with increasing welding speed at constant, low spindle speed, which resulted in high flow stress (cold welding conditions) and high weld pitch. The image on the right shows volumetric defects that presented as tearing of the weld crown surface and the presence of what appeared to be discrete fragments of material packed into the upper stir zone.

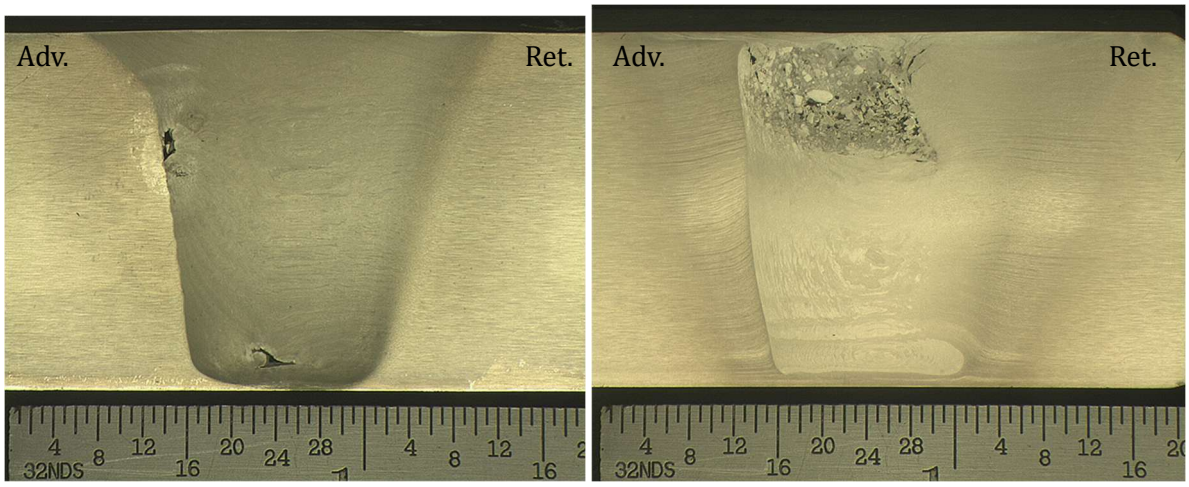

Figure 6. Transverse macro sections from 25.4-mm 7075-T6 FSW. (left) SZ boundary defects from cold welding conditions (90 rev/min spindle speed (0.10 m/s surface velocity) and 2.12 mm/s welding speed (1.42 mm/rev pitch)), (right) tearing defects from hot welding conditions (285 rev/min (0.30 m/s surface velocity) and 1.27 mm/s welding speed (0.27 mm/rev pitch)).

Figure 7 shows maps of welds made at CTC as a function of machine settings, derived from welding speed and spindle speed, with contours of constant flow stress overlaid. In the figure, weld quality is represented by red colored markers, denoting "demerits", which may include PAUT indications, volumetric defects detected from macro section inspections, low tensile strength or low tensile ductility. Weld sections that had only PAUT indications are denoted with pink colored markers. Green or blue markers represent conditions that had no demerits. These welds were made with constant shoulder contact conditions, as judged by the machine operator, thereby reducing the influence of shoulder pressure on the flow stress values.

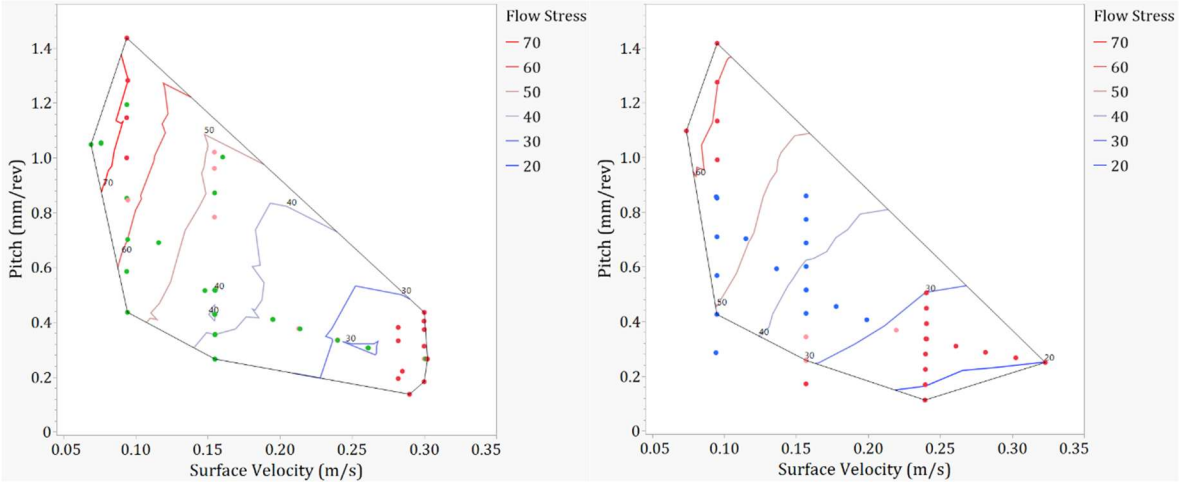

Figure 7. Contour plots of flow stress as a function of surface velocity and weld pitch, 12.7-mm 7075-T6 FSW (left) and 25.4-mm 7075-T6 FSW (right). Conditions for welding experiments shown as circular markers, red markers represent conditions with quality demerits, blue or green markers represent welding conditions without demerits, pink markers indicate PAUT quality demerit only.

Study of the maps in Figure 7 reveal patterns of defect formation with respect to machine settings and flow stress. Weld segments that had no demerits were approximately centered about the 40 MPa flow stress contour. Weld segments that had flow stress below 30 MPa generally had

volumetric defects resembling those presented on the right in Figure 6. These defects presented as "tearing" of the workpiece material, which could plausibly result from exceeding the hot workability of the base material in conditions of low flow stress, discussed further below. A second region of defect formation was observed at conditions of high flow stress and high weld pitch. These defects presented as what are commonly referred to as "wormhole" defects, shown for example in the right side of Figure 6. These defects resemble those produced early in the development of FSW at The Welding Institute (TWI), prior to the development of the threaded pin design. It is unclear if the root cause of these observed defects is use of a weld pitch that exceeds the capacity of the pin features, threads and flats in this case, to produce rotational transport that is sufficient to fill the space behind the pin on the advancing side, or if the root cause was simply very high flow stress that prevented coalescence of material on the advancing side of the stir zone behind the tool.

Three welding conditions made in 25.4-mm 7075 at moderate flow stress (around 50 MPa) exhibited PAUT indications and exhibited transverse tensile failures that originated in the stir zone, indicated with pink markers in the chart on the left in Figure 7 at a surface velocity of 0.15 m/s. This failure location is normally suggestive of a poorly formed stir zone that can be associated with low transverse ductility, but in this case the welds all had high transverse ductility and the very highest tensile strengths of all conditions tested. This phenomenon was also noted in unpublished welds in 25.4-mm 2519 aluminum made at high welding speed (1.7 mm/s). It appears that this combination of machine settings produced welds with HAZ strength that was simply higher than the strength of the stir zone, shifting the failure location. Apparently, the PAUT indications did not reflect actual defects but may have come from reflection of the ultrasonic signal from the resulting grain structure. The welds in 25.4-mm 2519 made at high welding speed all exhibited abnormal grain growth in the as-welded joints.

Energy density was also studied in relation to weld quality. As background, a rationalization of the relationship between energy density and temperature distribution is presented here. It can be shown, working from the Rosenthal solution for temperature distribution in a semi-infinite plate, that the energy density is proportional to the temperature distribution, as follows. The Rosenthal solution for the two-dimensional flow of heat [22] and a linear heat source is given by,

Equation 9. $$T - T_0 = \frac{q'}{2\pi} e^{-\lambda v \xi} K_o(\lambda v r),$$

where T is the temperature at a given distance from the heat source, T_0 is the initial temperature at that point, q' is the power output per unit length of heat source (essentially the workpiece thickness), κ is the thermal conductivity, $1/2\lambda$ is the thermal diffusivity, v is the welding speed, ξ is the distance from the heat source to the point of interest in the welding direction and r is the radial distance from the heat source to the point of interest. For a given workpiece material, material thickness and distance to the point of interest from the source of heating, the exponential and Bessel function terms reduce to approximately c/v as the welding speed increases, where c is a constant, as shown in Figure 8. For all values of welding speed, the trend of the product of the exponential term and the Bessel function term trends with 1/v and converges close to c/v at some sufficiently high welding speed.

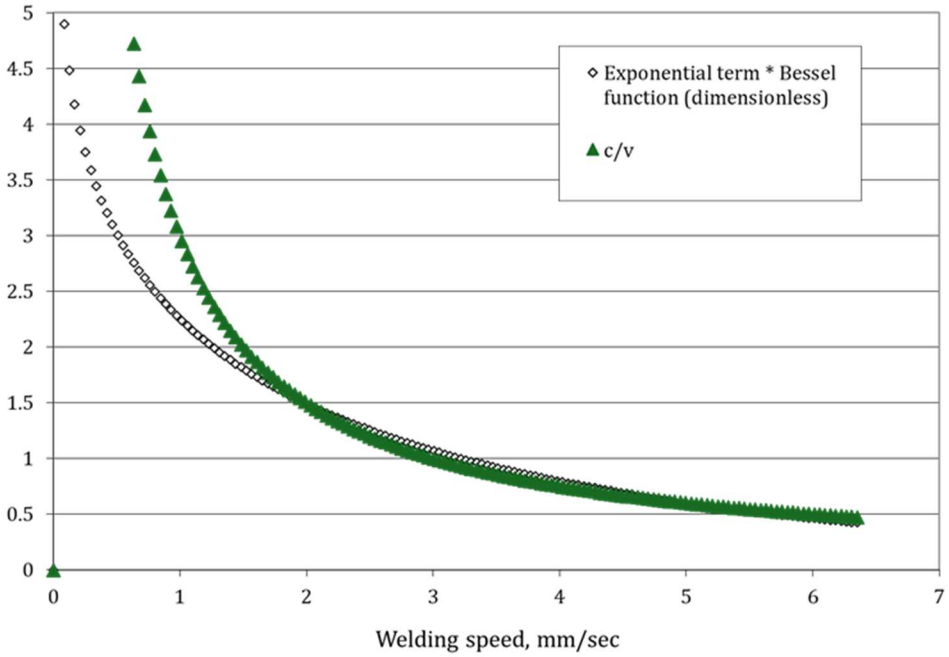

Figure 8. The product of the exponential and Bessel function terms in the Rosenthal solution as a function of welding speed. For v in units of mm/s and thermal properties of 5083 aluminum, for example, c = 3.

Then, for a given workpiece material (constant thermal properties), workpiece thickness, heat source power output and distance to the point of interest, the temperature distribution reduces to a proportionality given by,

Equation 10. $$T - T_0 \propto \frac{q'}{v} = \frac{\omega T}{v} = \frac{T}{pit} \propto \rho_E$$

Based on this, the temperature distribution surrounding the welding tool is directly proportional to the energy density for an infinite workpiece. This assumes a two-dimensional distribution of heat with no surface losses and is admittedly an idealization, but it is instructive of how energy density might relate to the transverse tensile strength of a welded joint. For example, higher energy density implies higher temperature distribution in the heat affected zone, where tensile failure typically originates in well-formed welds.

The correlation between energy density and transverse tensile strength of various aluminum alloys was studied using data from CTC's compiled FSW Data Set [23]. The FSW Data Set was started as a compilation of welding procedures from literature that represented details from welds that were reported to produce sound welds. This was initially used as a form of guidance for estimating tool designs and machine settings for new welding procedures and was regarded as being "better than nothing" in terms of a starting point for procedure development. CTC has expanded the Data Set to include unpublished results from internal projects and to include procedures with varying degrees of weld quality, along with ways to characterize deviations from "perfect" quality, referred to as demerits. The data set is available for public download [23].

Five cohorts of data from the Data Set included tensile strength data collected over ranges of machine settings. Plotting the data from these cohorts as a function of the ratio of weld strength to

parent metal strength for ultimate tensile strength (UTS) as a function of weld energy density is shown in Figure 9. Similar results were obtained for yield strength data from these welds. The effect of temperature distribution on tensile strength in these alloys is clearly represented in the trend of strength with respect to energy density for these diverse welding procedures. The implication is that higher energy density produces higher temperature distribution, leading to increased decrease in strength in the heat affected zone, where tensile failures typically occur in well-formed joints.

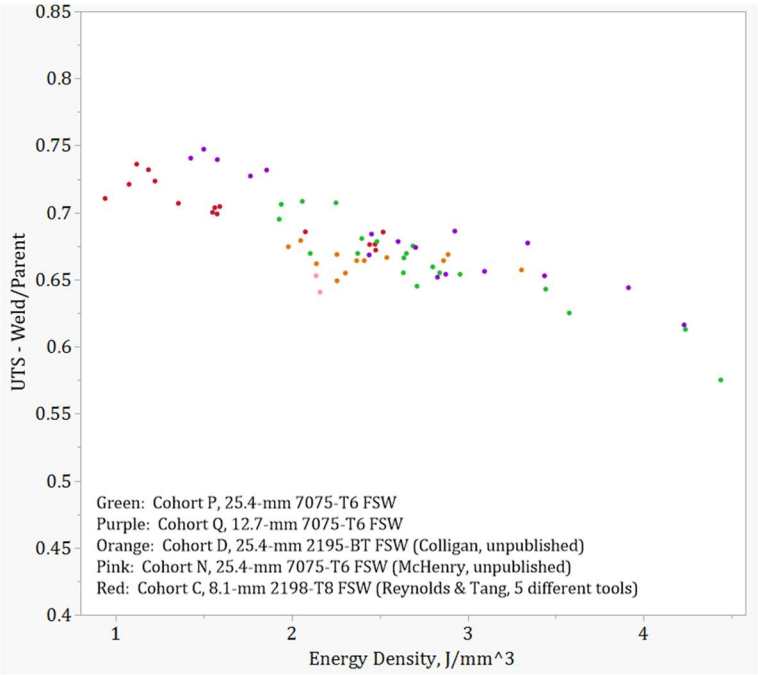

Figure 9. Ratio of base metal to weld transverse ultimate tensile strength as a function of energy density for various cohorts of data from the Data Set [23].

Discussion

This work demonstrated the role of two data features that relate to weld quality and transverse tensile properties, calculated from the basic tool geometries, machine settings and measured forces. Flow stress was shown to correlate with weld quality in terms of volumetric soundness. Although the data was not presented here, analysis of flow stress and transverse tensile properties did not show a correlation, except that within a middle range of flow stress all tensile results were high, and outside of that range the strength was low, entirely due to volumetric defects.

Volumetric defects produced under low flow stress conditions had a specific morphology that suggested fracture of workpiece material into fragments that were then deposited into the upper stir zone. Metals subjected to high temperature deformation are known to exhibit workability limits. Here, workability refers to "the ease with which a material can be shaped by plastic flow without the onset of fracture" [24]. Workability has two aspects: "intrinsic" workability refers to the response of the alloy chemistry to prior processing and "state-of-stress" workability refers to the response of the material to the imposed combination of strain, strain rate, flow stress and hydrostatic stress conditions. When the workability limit of a given material is exceeded, the material experiences fracture instead of plastic deformation, producing defects in hot-deformation processes such as forging and extrusion. Under conditions of low flow stress in FSW, the elevated

spindle speed results in high thermal softening and high "feature velocity", likely resulting in relatively high strain rate. Furthermore, in the area behind the pin there is likely to be low hydrostatic stress as a result of the forward progress of the tool. Hot workability principles indicate that these conditions favor fracture over plastic deformation, potentially leading to the defects observed at low flow stress as the welding tool features interact with the workpiece.

If hot workability is the root cause of FSW defects in conditions of low flow stress, the intrinsic workability component is significant in the context of the present discussion. The implication of intrinsic workability is that the flow stress quality threshold in conditions of low flow stress is dependent on the alloy and prior microstructure. Unpublished project work at CTC has shown that alloy 2050 aluminum-lithium welds in 75-mm thickness exhibited a flow stress quality threshold between 22.5 MPa and 20.4 MPa, significantly below the threshold observed in 7075 aluminum. Furthermore, it is possible that alloys known to exhibit good hot workability, necessary for enhanced extrusion characteristics, may also be found to have low flow stress quality threshold values, resulting in a wide weldability envelope with respect to spindle speed due to the tolerance for low flow stress. For flow stress quality thresholds to be useful for advanced welding control, the threshold value should be determined for each alloy and possibly for each general microstructure, i.e., rolled versus cast.

It is notable that, in the analysis of flow stress as a quality threshold, it appears that the threshold is independent of the machine settings that result in the threshold. Referring to the chart on the right in Figure 7, representing data from welds in 25.4-mm 7075-T6, the 30 MPa flow stress contour appears to represent an approximate threshold below which defects were observed. This contour is produced in welds from a range of spindle speed and welding speed, suggesting that the quality transition can occur at various machine settings which produce the threshold spindle torque. This independence is significant for using the flow stress as a control parameter for avoiding conditions that produce defects.

High flow stress was observed to coincide with defects of a very different morphology, commonly referred to as "wormhole" defects. Interestingly, the first attempts at FSW used welding tools that were smooth, without threads or flats. Those early experiments with FSW all exhibited wormhole defects. It wasn't until TWI introduced the threaded pin profile that sound welds could be produced. It is possible that weld defect correlation with conditions of high flow stress may also be fundamentally related to the weld pitch (travel/revolution) capacity of a given welding tool design. It is possible that as the weld pitch increases, the amount of material interacting with the pin features on each revolution exceeds the "pitch capacity" of the tool, causing it to produce defects that resemble those made with smooth welding tools. The present project has formulated a "pitch parameter" data feature, based on the weld pitch, the thread depth and the number of flats, to possibly describe a quality threshold for this type of defect, although additional work to confirm the method is needed.

Energy density was shown to correlate with tensile strength through its role in determining the temperature distribution, most notably in the region just outside the stir zone where tensile failures typically occur in well-formed welds. Analysis of energy density data on this program showed some correlation with the severity of defects produced but didn't demonstrate a quality threshold the way that flow stress did, since an energy density level that produced defects at high weld pitch did not produce defects at lower pitch values. This suggests that weld pitch is more likely the root cause of wormhole defects and not low energy density, implying that the quality threshold for wormhole

defects may be based on weld pitch and the tool design details such as the thread depth and the number of flats.

Weld power was not found to be useful as a basis for advanced welding controls due to its dependence on the heat conduction boundary conditions, even when converted to the unit-area equivalent of heat flux. It was generally found that weld power can be thought of as "how hard the process must work to achieve the conditions at the tool/workpiece interface". In experiments with variable boundary conditions, it was found that while holding constant flow stress during transition from a wide-plate boundary condition to a narrow, restricted boundary condition, the heat flux was markedly reduced [14]. This is simply because less power is needed to maintain constant torque, by manipulating machine settings, when the workpiece is narrowed. Alternatively, flow stress threshold values were found to be less dependent on boundary conditions and machine settings.

Based on this work, it is suggested that flow stress and energy density, calculated from spindle torque, the basic welding tool geometry, and machine settings, may be used as a basis for welding specifications. Flow stress and weld pitch appear to be key parameters for avoiding volumetric defects, while energy density is important for the control of weld strength. Based on the experiments in 7075-T6 FSW for materials between 12.7-mm and 25.4-mm thickness, welds with flow stress between 30 MPa and 58 MPa exhibited no volumetric defects. Based on this range, a flow stress control setpoint of about 40 MPa and a weld pitch target of about 0.5 mm/rev are expected to avoid the production of volumetric defects using welding tools with similar feature sizes to those tested here. Holding a fixed flow stress and weld pitch also has the effect of holding a constant energy density. Higher weld pitch values also produced sound welds with increasing tensile strength, although it is expected that a quality threshold related to high weld pitch exists.

It appears that the flow stress quality thresholds are potentially independent of the welding speed and spindle speed settings required to achieve the flow stress, which is important for conditions of variable boundary conditions where manipulation of machine settings is required to maintain constant flow stress. Based on the experimental results, it is possible that a welding specification based on a 40 MPa flow stress and 0.5 mm/rev weld pitch could be used to adaptively control welds in 7075-T6 plate in an application that presents variable weld boundary conditions. This adds another method of adaptively controlling the welding process, similar to the way that temperature control has been demonstrated in FSW. Work conducted on the use of flow stress and energy density to adaptively control FSW is reported in a separate paper [18].

Conclusions

Full penetration welds were made in 12.7-mm, 25.4-mm and 50.8-mm thick 7075-T6 aluminum plates using conventional FSW tools. For each weld, unit-area data features were calculated from the welding tool geometry, machine settings and measured process forces. Each weld was characterized with respect to weld quality using phased-array ultrasonic testing (PAUT), visual inspection of the crown surfaces, macro section examination and transverse tensile testing. The unit-area data features were analyzed in relation to the machine settings to establish empirical relationships and were also analyzed to isolate correlation with weld volumetric soundness and mechanical properties.

In this study it was found that flow stress could be described by empirical relations from linear regression analysis of welding speed, inverse surface velocity, shoulder pressure and weld pitch.

Good prediction was achieved using pooled results from welds in 25.4-mm and 50.8-mm plates, and from welds in 12.7-mm plates made at CTC and PAR Systems, although the prediction in 12.7-mm material was somewhat different from the prediction from the thicker materials. The method was also applied to continuous log file data from multiple welds with good agreement.

The analysis to correlate unit-area data features with weld strength and volumetric quality showed that flow stress was a critical indicator of weld volumetric quality, with welds exhibiting flow stress below a 30 MPa and above about 58 MPa thresholds having volumetric defects. Weld pitch may also play a role in the production of volumetric defects in high flow stress conditions. Energy density was shown to be related to the temperature distribution surrounding the point of welding. Of greatest interest is the temperature in the heat affected zone where tensile failures typically originate in well-formed welds. Not surprisingly, energy density was found to correlate with ultimate and yield tensile strength values. Heat flux, the unit-area expression of weld power, was not found to be useful in the prediction of volumetric defects or tensile properties.

Based on this work, flow stress and energy density unit-area data features, along with weld pitch, have been identified as the key for the development of adaptive welding controls. These controls were tested on welding equipment at PAR Systems and will be reported on in a subsequent paper [18]. Future work is required to establish flow stress quality threshold values for other alloys, workpiece thickness and initial microstructures and to establish a unit-area data feature that describes weld pitch capacity as a function of welding tool design.

References

1. Cederqvist, L., Bolsmjo, G. and Sorensen, C.D., "Adaptive control of novel welding process to seal canisters containing Sweden's nuclear waste using PID algorithms," Int'l. Conf. on Flex. Auto. And Intelligent Mfg., FAIM, Skovde, Sweden, 2008.
2. Fehrenbacher, A., Pfefferkorn, F.E., Zinn, M.R., Ferrier, N.J. and Duffie, N.A., "Closed-loop control of temperature in friction stir welding," 7th International Symposium on Friction Stir Welding, The Welding Institute, Cambridge, UK 20-22 May, 2008, Awaji Island, Japan.
3. Fehrenbacher, A., Duffie, N.A., Ferrier, N.J., Zinn, M.R. and Pfefferkorn, F.E., "Temperature measurement and closed-loop control in friction stir welding," 8th International Symposium on Friction Stir Welding, The Welding Institute, Cambridge, UK 18-20 May 2010, Timmendorfer Strand, Germany.
4. Mayfield, D.W. and Sorensen, C.D., "An improved temperature control algorithm for friction stir processing," 8th International Symposium on Friction Stir Welding, The Welding Institute, Cambridge, UK 18-20 May 2010, Timmendorfer Strand, Germany.
5. Cederqvist, L., Reynolds, A.P., Sorensen, C.D. and Garpinger, O., "Reliable FSW of copper canisters using improved process and regulator controlling power input and tool temperature," 8th International Symposium on Friction Stir Welding, 18-20 May 2010, Timmendorfer Strand, Germany.
6. Ross, K., "Investigation and implementation of a robust temperature control algorithm for friction stir welding," MS Thesis, Department of Mechanical Engineering, Brigham Young University, April 2012.
7. Arbegast, W.J., "Using process forces as a statistical process control tool for friction stir welding," Friction Stir Welding and Processing III, Eds. K.V. Jata, M.W. Mahoney, R.S. Mishra and T.J. Lienert, pp. 193-203, TMS, 2005.

8. Boldsaikhan, E., Corwin, E., Logar, A. and Argegast, W., "Neural network evaluation of weld quality using FSW feedback data," 6th International Symposium on Friction Stir Welding, Montreal, 2006.
9. Jene, Tobias, et al. "Monitoring of the friction stir welding process to describe parameter effects on joint quality," Welding in the World, 52(9), pp. 47-53, 2008.
10. Boldsaikhan, E., Corwin, E. and Arbegast, W., "Detecting wormholes in friction stir welds from welding feedback data," Proceeding of the 42nd Midwest Instruction and Computing Symposium (MICS 2009), Rapid City, SD, US, 2009.
11. Hunt, J.B., Mazzeo, B.A., Sorensen, C.D. and Hovanski, Y., "A generalized method for in-process defect detection in friction stir welding," Journal of Manufacturing and Materials Processing, 6(80), 2022.
12. Colligan, K., "Analysis of data from friction stir welds in aluminum," Presented at the Joint International Symposium on Friction Stir Welding and Processing, The Welding Institute, Cambridge, UK, Luneburg, Germany, 28-30 September 2022.
13. Colligan, K., "Analysis of torque data from friction stir welds in aluminum alloys," Friction Stir Welding and Processing XII, TMS (the Minerals, Metals and Materials Society), pp. 75-85, 2023.
14. Colligan, K., "Unit-area analysis of friction stir welding data," Presented at the 13th International Symposium on Friction Stir Welding and Processing, The Welding Institute, Cambridge, UK, Kyoto, Japan, 21-23 May, 2024.
15. Colligan, K., "Analysis of FSW macro-sections in aluminum relative to unit-area analysis," Friction Stir Welding and Processing XIII, TMS (the Minerals, Metals and Materials Society), pp. 215-232.
16. Rodrigues, D.M., Leitao, C., Louro, R., Gouveia, H. and Loureiro, A., "High speed friction stir welding of aluminum alloys," Science and Technology of Welding and Joining, 2010.
17. Liu, X., Gerlich, A.P. and Mendez, P.F., "Process envelope and void defect analysis in FSW of AA2024, AA5052 and AA7075 aluminum alloys," Science and Technology of Welding and Joining, 2025, 13621718251413024.
18. Colligan, K. and Hunt, J., "Automatic Adaptive Control of Friction Stir Welding," 14th International Symposium on Friction Stir Welding, The Welding Institute, Cambridge, UK, Cambridge, UK, 19-21 May, 2026.
19. Andrade, D.G., Leitao, C., Dialami, N., Chiumenti, M. and Rodrigues, D.M., "Modelling Torque and Temperature in Friction Stir Welding of Aluminum," Int. Journal of Mechanical Sciences, Vol. 182, 16 May, 2020.
20. Schmidt, H., Hattel, J. and Wert, J., "An analytic model for the heat generation in friction stir welding," Modelling and Simulation in Materials Science and Engineering, 2004, Vol. 12, pp. 143-157.
21. Reynolds, A.P. and Tang, W., "Alloy, tool geometry and process parameter effects on friction stir weld energies and resultant FSW joint properties," Friction Stir Welding and Processing, TMS, 4-8 November 2001, Indianapolis, IN, pp. 15-23.
22. Rosenthal, D., "The theory of moving sources of heat and its application to metal treatments," Welding Journal, American Welding Society, 1946.
23. https://www.ctc.com/friction-stir-welding.aspx
24. Prassad, Y.V.R.K. (ed) (2015) Hot working guide, 2nd edition, ASM International, Materials Park, OH.